J Mater Sci (2006) 41:8001–8012
DOI 10.1007/s10853-006-0869-y

Structural, photophysical and photocatalytic properties of Bi_2MTaO_7 (M = La and Y)

Jing-Fei Luan · Xi-Ping Hao · Shou-Rong Zheng · Guo-You Luan · Xiao-Shan Wu

Received: 2 August 2005 / Accepted: 4 November 2005 / Published online: 21 September 2006

Abstract Bi_2MTaO_7 (M = Y and La) were synthesized by solid-state reaction method and their structural and photocatalytic properties were investigated. The results indicated that these compounds crystallize in the pyrochlore-type structure, cubic system with space group Fd-3 m. In addition, the band gaps of Bi_2LaTaO_7 and Bi_2YTaO_7 were estimated to be about 2.17(3) and 2.22(7) eV, respectively. For the photocatalytic water splitting reaction, H_2 or O_2 evolution was observed from pure water respectively with Bi_2MTaO_7 (M = Y and La) as the photocatalysts under ultraviolet light irradiation. Photocatalytic degradation of aqueous methylene blue (MB) dye over these compounds was further investigated under visible light irradiation. Bi_2MTaO_7 (M = Y and La) showed markedly higher catalytic activity compared to P-25 for MB photocatalytic degradation under visible light irradiation. Complete removal of aqueous MB was observed after visible light irradiation for 190 min with Bi_2LaTaO_7 as the photocatalyst and for 200 min with Bi_2YTaO_7 as the photocatalyst. The decrease of the total organic carbon (TOC) and the formation of inorganic products, SO_4^{2-} and NO_3^-, demonstrated the continuous mineralization of aqueous MB during the photocatalytic process.

J.-F. Luan (✉)
State Key Laboratory of Pollution Control and Resource Reuse, School of Environment, Nanjing University, Nanjing 210093, People's Republic of China
e-mail: jfluan@nju.edu.cn

X.-P. Hao
Department of Materials Science and Engineering, National Laboratory of Solid State Microstructures, Nanjing University, Nanjing 210093, People's Republic of China

S.-R. Zheng
State Key Laboratory of Pollution Control and Resource Reuse, School of Environment, Nanjing University, Nanjing 210093, People's Republic of China

G.-Y. Luan
State Key Laboratory of Catalysis, Dalian Institute of Chemical Physics, Chinese Academy of Sciences, Dalian 116023, People's Republic of China

X.-S. Wu
National Laboratory of Solid State Microstructures, Nanjing University, Nanjing 210093, People's Republic of China

Introduction

Since Honda and Fujishima first observed the splitting of water on TiO_2 electrode in 1972 [1], the semiconductor based photocatalytic process has attracted extensive attention from both academic and industrial societies [2, 3]. The photocatalytic water splitting using solar energy to produce H_2 is of special significance due to the urgent demand of clean and renewable sources [2–4]. Up to now, a variety of photocatalysts with different structures have been synthesized to explore the highly effective utilization of solar energy [5–9]. Among them, some Nb-containing photocatalysts with a pyrochlore-type structure were reported recently, such as Bi_2MNbO_7 (M = Al, Ga, In and Fe) [10] and Bi_2RNbO_7 (R = Y, rare earth elements) [11]. Ta-containing semiconductor oxides generally show a higher photocatalytic activity than their Nb-containing counterparts, which has been proved by the results of $Sr_2M_2O_7$ [12] and $InMO_4$ (M = Nb and Ta) [13].

In addition, scientific interest in the photocatalytic degradation of aqueous organic pollutants has quickly increased recently [14–16]. In particular, it was reported that 15% of the total world production of dyes is lost during the dyeing process and is released to the textile effluents, which eventually pollute the groundwater. The release of those colored waste waters in the ecosystem is a dramatic source of non-aesthetic pollution, eutrophication and perturbations in the aquatic life. Many reports have revealed that the organic dyes could be effectively degraded using the TiO_2-based photocatalytic process; however, the degradation of a majority of organic dyes are only under UV irradiation except for some dyes, such as alizarin red, which can be degraded under visible light using the TiO_2-based photocatalysts based on the dye-sensitized process [17, 18]. Among different dyes, methylene blue dye (MB) is difficult to be decomposed under visible light irradiation and is usually regarded as a model dye contaminant to evaluate the activity of a photocatalyst [19, 20]. Up to now, there were only few reports of MB dye degradation under visible light irradiation [19, 21]. Therefore, it is highly desirable to develop new visible light-driven photocatalysts with high activity.

Among the rare earth compounds, the strongly localized f-shell that is often described as a core-like shell influences the chemical and physical properties of the lanthanides [22]. The performance change of the lanthanides usually has a monotonic character [23]. It has been generally observed that numerous compounds with the $A_2B_2O_7$ pyrochlore structure display antiferroelectric phases or dielectric abnormality. However, only a few compounds display ferroelectric behavior [24, 25]. Bi_2MTaO_7 (M = Y and La) belongs to the family of the $A_2B_2O_7$ compounds, but the data about its space group and lattice constants have not been reported previously. Moreover, no photocatalytic properties of Bi_2MTaO_7 (M = Y and La) have been investigated so far. We considered that Y^{3+} or La^{3+} occupying the B site and Bi^{3+} occupying the A site in the $A_2^{3+}B_2^{4+}O_7$ compounds may lead to an increase in hole (carrier) concentration, and thus result in a change in the electrical transportation and photophysical properties. We also speculate that Bi_2MTaO_7 (M = Y and La) might yield a slight modification of crystal structure and result in a change in photophysical properties. It is noteworthy that a slight modification in the structure of a semiconductor will lead to a marked change in photocatalytic properties [15]. In this contribution, we prepared the Bi_2MTaO_7 (M = Y and La) photocatalysts and the structural and photocatalytic properties of Bi_2MTaO_7 (M = Y and La) were studied in detail. A comparison of the photocatalytic property of Bi_2MTaO_7 (M = Y and La) with that of TiO_2 (P-25) is also provided.

Experimental procedure

The polycrystalline samples of the photocatalysts were synthesized by a solid-state reaction method. La_2O_3, Y_2O_3, Bi_2O_3 and Ta_2O_5 with purity of 99.99% were used as starting materials. The powders were dried at 200 °C for 4 h. The stoichiometric amounts of precursors were mixed and pressed into small columns. At last the small columns were sintered at 1080 °C for 52 h in an alumina crucible with an electric furnace. The crystal structure of Bi_2MTaO_7 (M = Y and La) were analyzed by the powder X-ray diffraction method with CuK_α radiation ($\lambda = 1.54056$). The data were collected at 295 K with a step scan procedure in the range of $2\theta = 5$–$100°$. The step interval was 0.02° and the scan speed was $1°min^{-1}$. The chemical composition of the compound was determined by scanning electron microscope-X-ray energy dispersion spectrum (SEM-EDX) and X-ray Fluorescence spectrometer (ARL-9800). The optical absorption of Bi_2MTaO_7 (M = Y and La) were analyzed with an UV–visible spectrophotometer (Lambda 35). The surface areas were determined using the BET method with N_2 adsorption at liquid nitrogen temperature.

The photocatalytic degradation of aqueous MB was performed with 0.5 g Bi_2YTaO_7 or Bi_2LaTaO_7 powders suspended in 100 mL methylene blue solution (MB solution concentration was 0.0506 mol m^{-3} and the initial pH value of the solution was 7) in a pyrex glass cell. The photocatalytic reaction system consisted of a 300 W Xe arc lamp and a cut-off filter ($\lambda > 420$ nm). The concentration of MB was determined with a UV–vis spectrometer (Helios Beta) with the detecting wavenumber at 670 nm. The inorganic products of MB degradation were detected by ion chromatograph (DX-300). Total organic carbon (TOC) was determined with a TOC analyzer (model TOC-5000).

The photocatalytic water splitting with Bi_2MTaO_7 (M = Y and La) as the photocatalysts was carried out in pure water (1.0 g powder catalyst, 300 mL H_2O) under UV irradiation. The catalysts were suspended in pure water by a magnetic stirrer and the photocatalytic reaction was conducted in a gas closed circulation system with an inner-irradiation type quartz cell and a 400 W high-pressure Hg lamp.

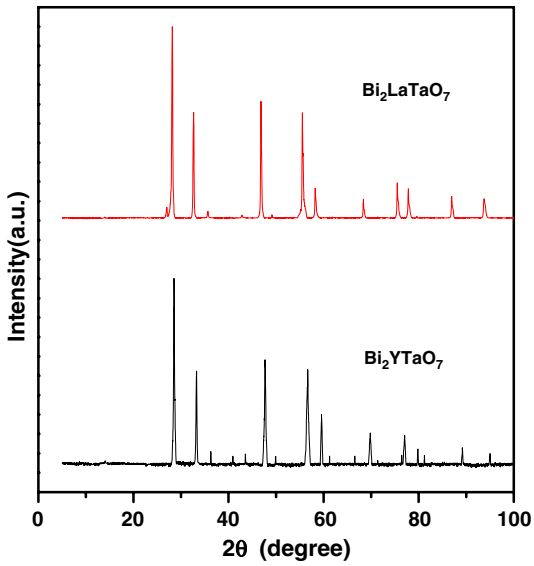

Fig. 1 X-ray powder diffraction patterns of the Bi_2MTaO_7 (M = Y and La) photocatalysts at 1080 °C

Results and discussion

Structural properties

Figure 1 shows X-ray diffraction patterns of Bi_2MTaO_7 (M = Y and La) sintered at 1080 °C in air. Figures 2 and 3 show SEM image and SEM-EDX spectra of Bi_2MTaO_7 (M = Y and La). The powder X-ray diffraction analysis showed that Bi_2MTaO_7 (M = Y and La) are single phase, which is consistent with the results from SEM-EDX. The chemical composition of the compound was determined using characteristic X-rays of Bi M_α and Ta L_α with the ZAF (element number, absorption and fluorescence corrections) quantification method. The SEM-EDX analysis revealed that Bi_2MTaO_7 (M = Y and La) had a homogenous atomic distribution with no other impure elements. An average atomic rate of Bi: La: Ta = 2.00: 0.97: 1.02 for Bi_2LaTaO_7 and Bi: Y: Ta = 2.00: 0.98:

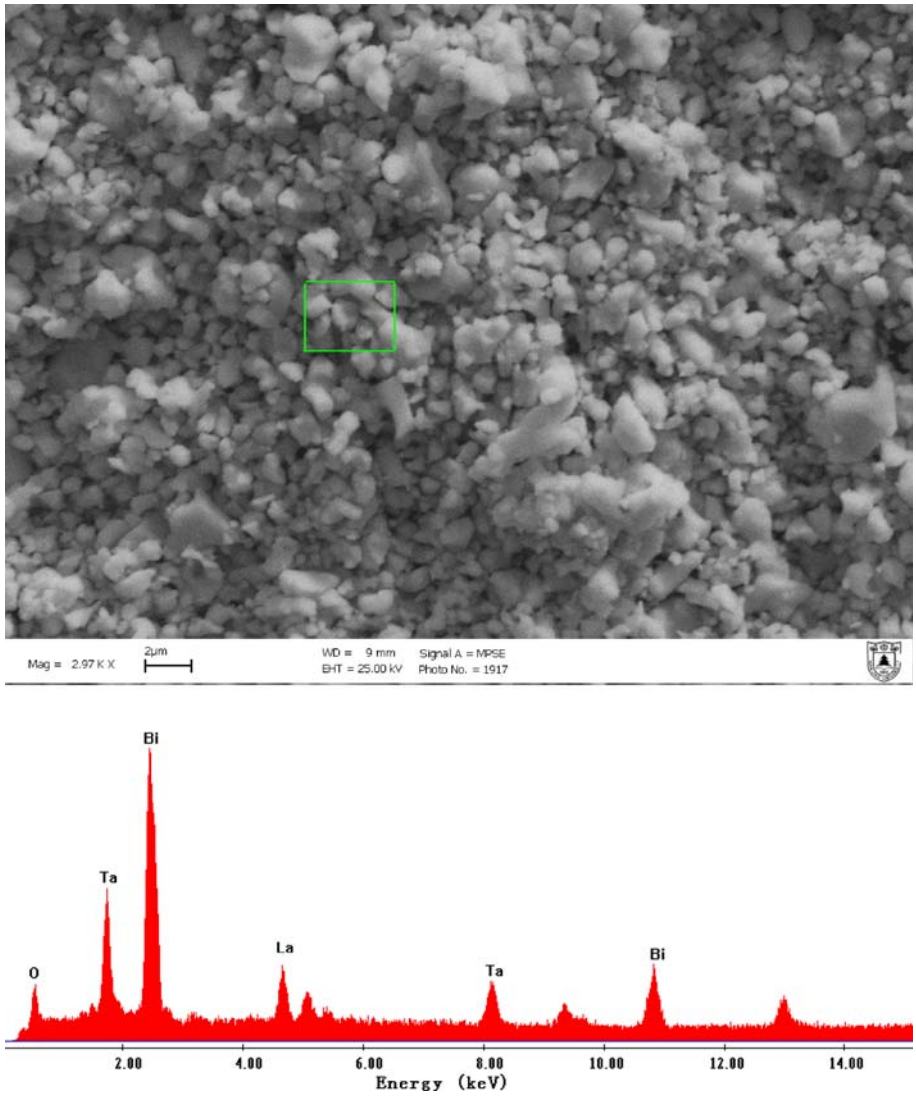

Fig. 2 SEM image and SEM-EDX spectrum taken from Bi_2LaTaO_7

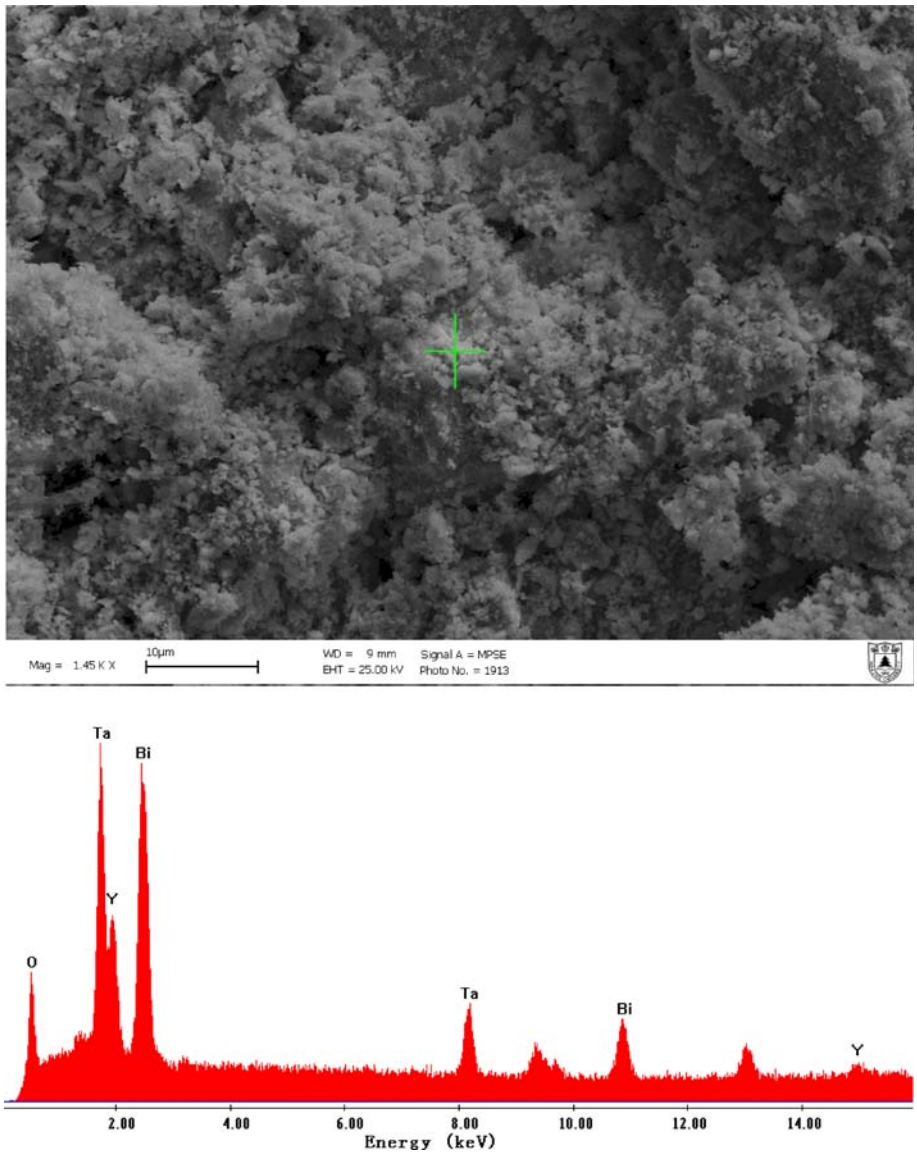

Fig. 3 SEM image and SEM-EDX spectrum taken from Bi_2YTaO_7

1.03 for Bi_2YTaO_7 was obtained from measurements at different points. The results are in good agreement with the measurement from X-ray Fluorescence spectrometer. Based on above results, we can conclude that the resulting materials are of high purity under our preparation conditions.

Full-profile structure refinement of the collected powder diffraction data for Bi_2MTaO_7 (M = Y and La) was conducted using the Rietveld program REITAN [26], by which positional parameters and isotropic thermal parameters of Bi_2MTaO_7 (M = Y and La) were refined. The refinement result of Bi_2LaTaO_7 is shown in Fig. 4 and the structure of Bi_2MTaO_7 (M = Y and La) is shown in Fig. 5. Bi_2MTaO_7 (M = Y and La) is consisted of the three-dimensional network of MO_6 (M = Ta, Y, La), stacked along [101] and separated by a unit cell translation (10.9600(2) or 10.7859(9) Å). The atomic coordinates and isotropic thermal parameters of Bi_2MTaO_7 (M = Y and La) are listed in Tables 1 and 2. The result of the final refinement for Bi_2MTaO_7 (M = Y and La) indicated a good agreement between the observed and calculated intensities in the pyrochlore type crystal structure of the cubic system with space group Fd-3m when the O atoms are included in the model. The lattice parameter is found to be a = 10.9600(2) Å for Bi_2LaTaO_7 and a = 10.7859(9) Å for Bi_2YTaO_7. All the diffraction peaks for Bi_2MTaO_7 (M = Y and La) could be successfully indexed based on the lattice constant and the space group mentioned above. Our X-ray diffraction results shows that Bi_2LaTaO_7 and Bi_2YTaO_7 crystallize in the same structure, and 2θ angles of each reflection of Bi_2LaTaO_7 change with La^{3+} being substituted by Y^{3+}. The lattice parameter decrease from a = 10.9600(2) Å for Bi_2LaTaO_7 to a = 10.7859(9) Å

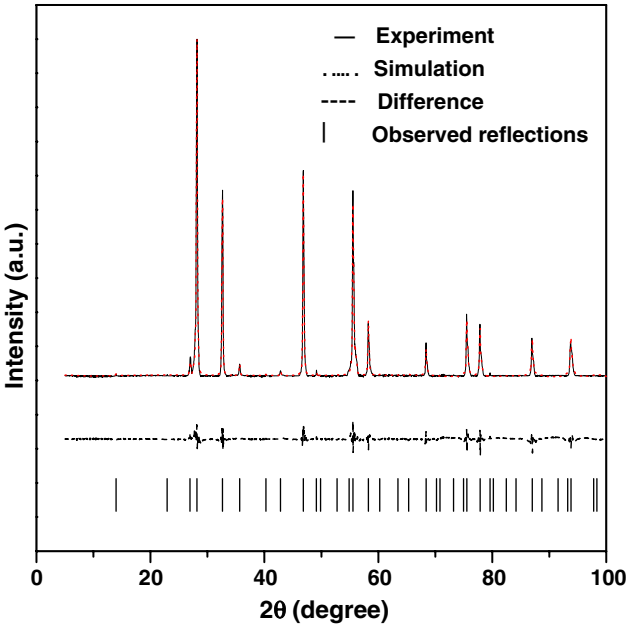

Fig. 4 Rietveld refinement of XRD data for the cubic Bi_2LaTaO_7 photocatalyst by a solid state reaction method at 1,080 °C. A difference (observed–calculated) profile is shown beneath. The tic marks represent reflection positions. The dot line represents simulation X-ray diffraction pattern (…). The beeline represents experimental X-ray diffraction pattern (—)

for Bi_2YTaO_7, which indicates a decrease in lattice parameter of the photocatalyst with decrease of the M ionic radii, Y^{3+} (0.90 Å) < La^{3+} (1.03 Å). The outcome of refinements for Bi_2LaTaO_7 generated the unweighted R factor, R_P = 9.88% in space group Fd3m when the O atoms are included in the model. Bernard [24] studied Bi_2CrNbO_7, Bi_2InNbO_7 and Bi_2FeSbO_7 and also observed the large R factors. Zou et al. [4] refined the crystal structure of Bi_2InNbO_7 and obtained a large R factor for Bi_2InNbO_7, which was ascribed to a slightly modified structure model for Bi_2InNbO_7. Note that the precursors with high purity were used in this study. The influence of minor impurities on the structure of Bi_2LaTaO_7 can be excluded, which was further supported by the fact that no impurities were detected by EDX analysis. Therefore, we speculate that the slight high R factor for Bi_2LaTaO_7 is resulted from a slightly modified structure model for Bi_2LaTaO_7. It should be emphasized that the defects or the disorder/order of a fraction of the atoms can lead to the change of structures, including different bond-distance distributions, thermal displacement parameters and/or occupation factors for some of the atoms [27].

Photophysical properties

Figure 6 shows the results of diffuse reflection spectra of the cubic Bi_2MTaO_7 (M = Y and La) photocatalysts. An average absorption of less than 5% was obtained from 500 nm to 800 nm. In contrast to the well-known TiO_2 whose absorption edge is at about 400 nm, the newly synthesized Bi_2MTaO_7 (M = Y and La) photocatalysts showed obvious absorption in visible light region up to 590 nm, which indicates that Bi_2MTaO_7 (M = Y and La) have the ability to respond to visible light.

For a crystalline semiconductor, it is commonly accepted that the optical absorption near the band edge follows the equation [28, 29]: $\alpha h\nu = A(h\nu\text{-}E_g)^n$. A, α, E_g and ν are proportional constant, absorption coefficient, band gap, and light frequency, respectively. Within this equation, n determines the character of the transition in a semiconductor. E_g and n can be calculated by the following steps: plot $\ln(\alpha h\nu)$ versus $\ln(h\nu - E_g)$ with an approximate value of E_g, then decide the value of n with the slope of the straightest line near the band edge, at last, plot $(\alpha h\nu)^{1/n}$ versus $h\nu$ and evaluate the band gap E_g by extrapolating the straightest line to the $h\nu$ axis intercept. Based on above method, the value of n for Bi_2MTaO_7 (M = Y and La) was calculated to be 0.5 from Fig. 6, indicating that the optical transitions for these oxides are directly allowed. Figure 7 shows the Plot of $(\alpha h\nu)^2$ versus $h\nu$ for Bi_2YTaO_7. It can be seen from Fig. 7 that Bi_2YTaO_7 own two bandgaps, which are consistent with those two band-edges in Fig. 6. It is noteworthy that the band gaps of Bi_2LaTaO_7 and Bi_2YTaO_7 are estimated to be 2.17(3) and 2.22(7) eV, indicating narrower band gaps compared to that of Bi_2InTaO_7 (2.9 eV [30]). This may imply that the photoabsorption of Bi_2MTaO_7 (M = Y and La) is stronger than that of Bi_2InTaO_7, which may result in a higher photocatalytic activity of Bi_2MTaO_7 (M = Y and La) than that of Bi_2InTaO_7. In principle, the photoabsorption of the photocatalyst depends on the mobility of electron–hole pairs, which determines the probability of electrons and holes to reach reaction sites on the surface of the photocatalyst. Figure 5 showed that Bi_2MTaO_7 (M = Y and La) consisted of the network of MO_6, which is built by forming infinite corner-sharing MO_6 octahedra with the zigzag chains along $[11\bar{1}]$. This suggests that photogenerated electron–hole pairs in the Bi_2MTaO_7 (M = Y and La) photocatalysts can move easily in this direction, which may result in a high photocatalytic activities of Bi_2MTaO_7 (M = Y and La).

Photocatalytic degradation of methylene blue

MB degradation with the Bi_2MTaO_7 (M = Y and La) or TiO_2 (P-25) as the photocatalysts under visible light irradiation ($\lambda > 420$ nm) are shown in Fig. 8. The

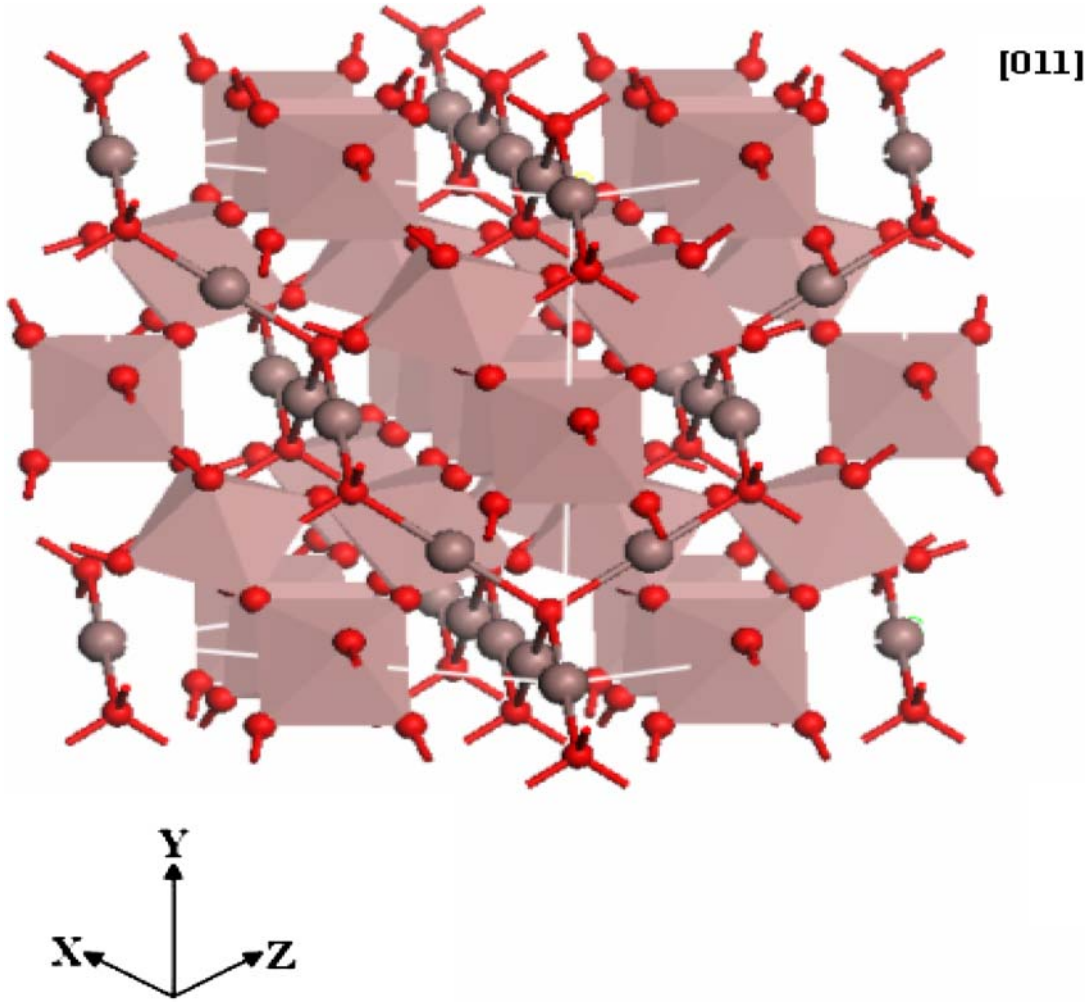

Fig. 5 The schematic structural diagram of the cubic Bi_2MTaO_7 (M = Y and La) photocatalysts. Three-dimensional network of MO_6 stacked along [101] and separated by a unit cell translation

Table 1 Structural parameters of Bi_2YTaO_7 prepared by solid state reaction method

Atom	*x*	*y*	*z*	Beq	Occupation factor
Bi	0.0000	0.0000	0.0000	2.915	1.0
Y	0.5000	0.5000	0.5000	0.464	0.5
Ta	0.5000	0.5000	0.5000	0.500	0.5
O(1)	–0.0947	0.1250	0.1250	1.000	1.0
O(2)	0.1250	0.1250	0.1250	1.000	1.0

Table 2 Structural parameters of Bi_2LaTaO_7 prepared by solid state reaction method

Atom	*x*	*y*	*z*	Beq	Occupation factor
Bi	0.0000	0.0000	0.0000	2.915	1.0
La	0.5000	0.5000	0.5000	0.464	0.5
Ta	0.5000	0.5000	0.5000	0.500	0.5
O(1)	–0.1957	0.1250	0.1250	1.000	1.0
O(2)	0.1250	0.1250	0.1250	1.000	1.0

results showed that the solution color changed from deep blue to colorless and MB concentration in the solution decreased to 0 mol m^{-3} after visible light irradiation for 190 min with the Bi_2LaTaO_7 as the photocatalyst. The initial rate of MB degradation was about 4.439×10^{-6} mol s^{-1} m^{-3}. Simultaneously, a SO_4^{2-}

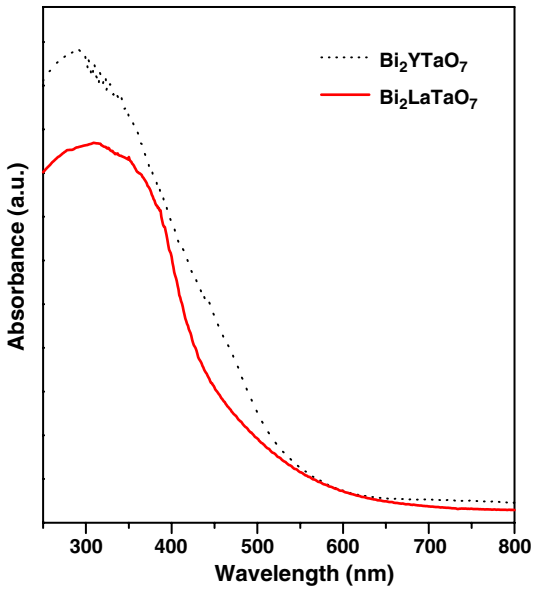

Fig. 6 Diffuse reflection spectrum of the cubic Bi_2MTaO_7 (M = Y and La) photocatalysts prepared by a solid state reaction method

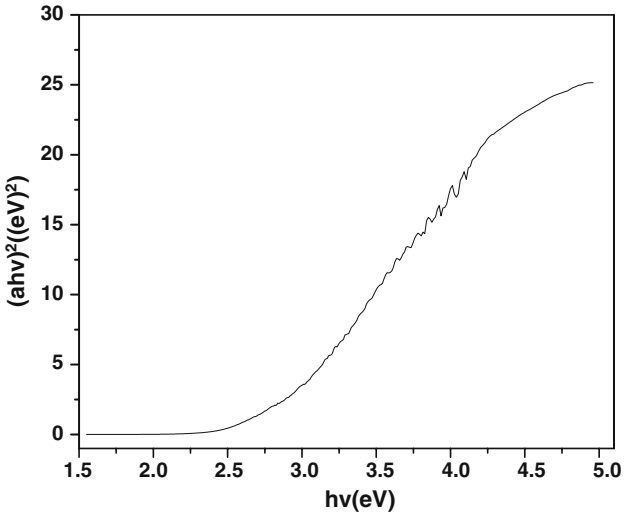

Fig. 7 Plot of $(\alpha h\nu)^2$ versus $h\nu$ for Bi_2YTaO_7

ion concentration of 0.0313 mol m^{-3} was detected in the solution after the photocatalytic reaction for 190 min, indicating that 61.9% of sulfur from MB was converted into sulfate ion. It was clear that aqueous MB was mainly mineralized rather than bleached under our experimental conditions. The catalytic quantum yield is defined as the ratio of the number of molecules transformed per second to the number of incident efficient photons (i.e. absorbable by Bi_2LaTaO_7) per second. If we assume that the conversion of a MB molecule only needs a photon, the resulting initial photocatalytic quantum yield was estimated to be 0.11% with an interference filter (λ = 420 nm) in the presence of the Bi_2LaTaO_7 photocatalyst.

The results also showed that MB concentration in the solution decreased to 0 mol m^{-3} after visible light irradiation for 200 min with Bi_2YTaO_7 as the photocatalyst. The initial rate of MB degradation was 4.217×10^{-6} mol s^{-1} m^{-3} and a SO_4^{2-} ion concentration of 0.0298 mol m^{-3} was detected in the solution after the photocatalytic reaction, indicating that 58.9% of sulfur from MB was converted into sulfate ion. The resulting initial photocatalytic quantum yield was estimated to be 0.10% with an interference filter (λ = 420 nm) for the Bi_2YTaO_7 photocatalyst.

In comparison, aqueous MB concentration decreased only from 0.0506 mol m^{-3} to 0.0355 mol m^{-3} after visible light irradiation for 200 min with TiO_2 as the catalyst, and no SO_4^{2-} ion was detected in the solution after the photo-reaction. Photobleaching of MB (MB photolysis) in the absence of catalyst was also carried out under visible light irradiation, as shown in Fig. 8. The result indicated that the rate of MB photolysis was almost the same as that of MB degradation with TiO_2 as the catalyst, suggesting that TiO_2 was completely inactive to MB photocatalytic degradation under visible light irradiation [14].

The ultimate aim of the photodegradation of organic pollutants is to completely convert the toxic organic compounds into inorganics, such as CO_2, SO_4^{2-} or NO_3^-, et al.. In the presence of Bi_2MTaO_7 (M = Y and La), the dependence of MB degradation products on the irradiation time is compared in Fig. 9. It can be seen that the concentration of SO_4^{2-} or NO_3^- ions increases with the increase of irradiation time. Note that the amount of SO_4^{2-} ions released into the solution is lower than that expected from stoichiometry. The first possible reason is the loss of sulfur-containing volatile compounds such as H_2S or SO_2. The second probable explanation is given by the partially irreversible adsorption of some SO_4^{2-} ions on the surface of the photocatalyst as already observed [31]. However, the partial irreversible adsorption of SO_4^{2-} ions does not restrain the photocatalytic degradation of pollutants [31]. The higher amount of NO_3^- ions is owing to the stoichiometric ratio $N/S = 3$ in the initial MB molecule.

In order to monitor whether MB is mineralized or not, the total organic carbon (TOC) was followed during visible light irradiation and the result is shown in Fig. 10. The results showed that in the absence of catalyst 29.8% of TOC decrease was obtained after visible light irradiation for 200 min. On the contrary, in the presence of Bi_2LaTaO_7, a significantly enhanced decrease of the TOC (96.1%) was obtained after 200 min of visible light irradiation. Consequently, the

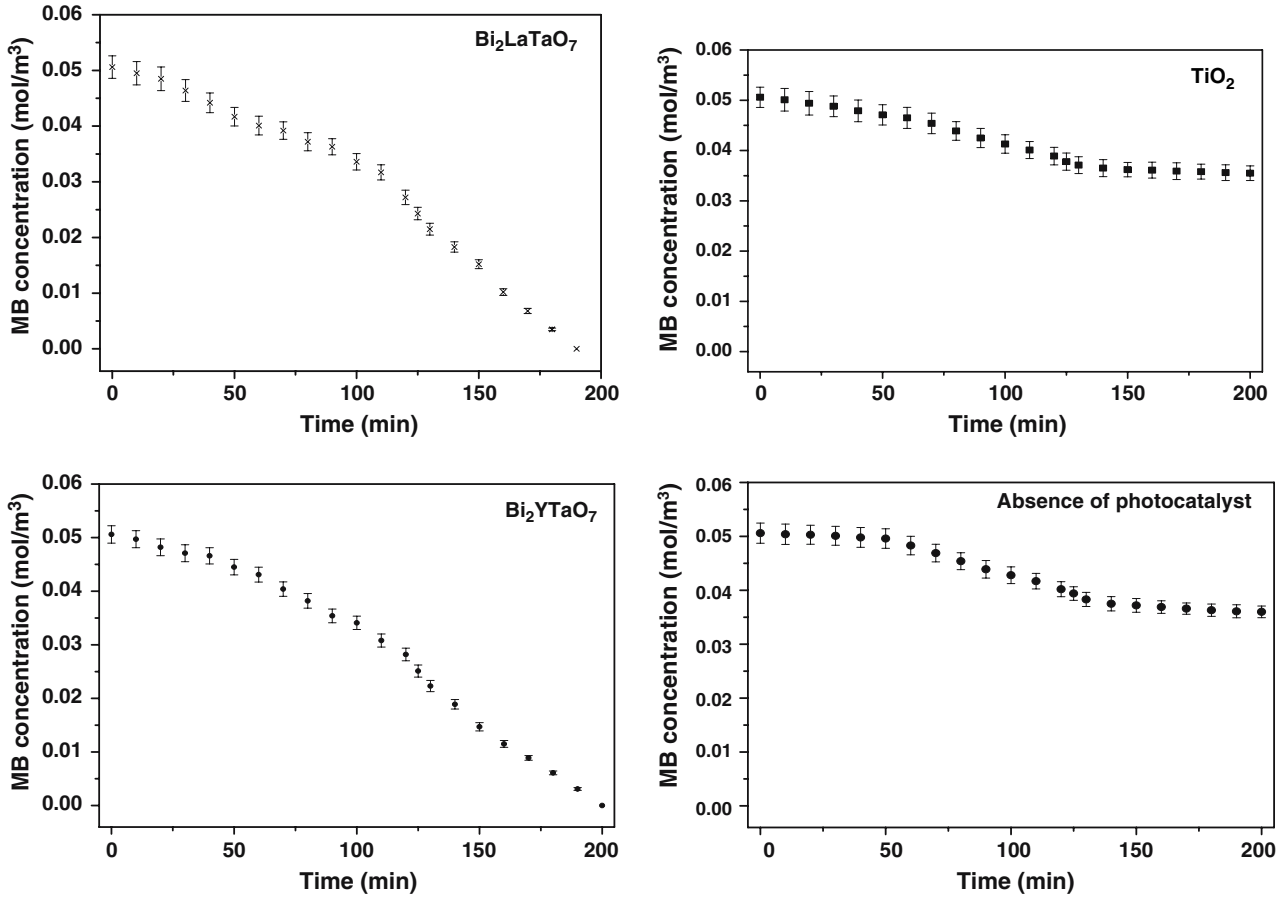

Fig. 8 Photocatalytic methylene blue degradation under visible light irradiation at room temperature in air for 200 min in the presence of Bi_2MTaO_7 (M = Y and La) and TiO_2 (P-25), as well as MB photolysis

complete mineralization of MB was achieved after 220 min of visible light irradiation in the presence Bi_2LaTaO_7. Similarly, we also found a decrease of TOC by 91.2% after 200 min of visible light irradiation with Bi_2YTaO_7 as the photocatalyst.

Photocatalytic water splitting

Figure 11 shows the photocatalytic H_2 evolution from pure water under UV light irradiation over the Bi_2MTaO_7 (M = Y and La) photocatalysts. H_2 evolution rates and some physical properties are listed in Table 3. It can be seen from Fig. 11 that the activities of Bi_2MTaO_7 (M = Y and La) are different and the results are listed in Table 3. It was found that H_2 evolution rates are estimated to be 41.8 μmol h^{-1} for Bi_2LaTaO_7 and 33.6 μmol h^{-1} for Bi_2YTaO_7, indicating that Bi_2LaTaO_7 exhibits a larger activity than Bi_2YTaO_7. The influence of the UV light irradiation was also investigated by light on/off shutter studies over Bi_2MTaO_7 (M = Y and La). The H_2 evolutions stopped by terminating the UV light irradiations, indicating that the reactions of H_2 evolutions were initiated by UV light irradiation. In the second run, almost the same H_2 evolution rate was obtained after the system was evacuated. Fig. 12 shows the photocatalytic O_2 evolution from pure water under UV light irradiation over the Bi_2MTaO_7 (M = Y and La) photocatalysts and the results are described in Table 3. Similar to H_2 evolutions, the O_2 evolutions increased with illumination time and O_2 evolution rates also varied according to the following order: $Bi_2LaTaO_7 > Bi_2YTaO_7$. In order to compare the catalytic activities of Bi_2MTaO_7 (M = La and Y) with that of TiO_2, water splitting with P25 as the catalyst was conducted. In the presence of P25, the rate of H_2 evolution from pure water was about 1.4 μmol h^{-1} in the first 15 h, which shows much lower activity than that of Bi_2MTaO_7 (M = La and Y).

Based on the observed H_2 and O_2 evolution from pure water, it can be concluded that the lowest conduction band level of Bi_2MTaO_7 (M = Y and La) are more negative than that of H_2 evolution and the highest valence band level are more positive than that of O_2 evolution. Namely, Bi_2MTaO_7 (M = Y and La) have proper band structures for the reduction of H^+ to

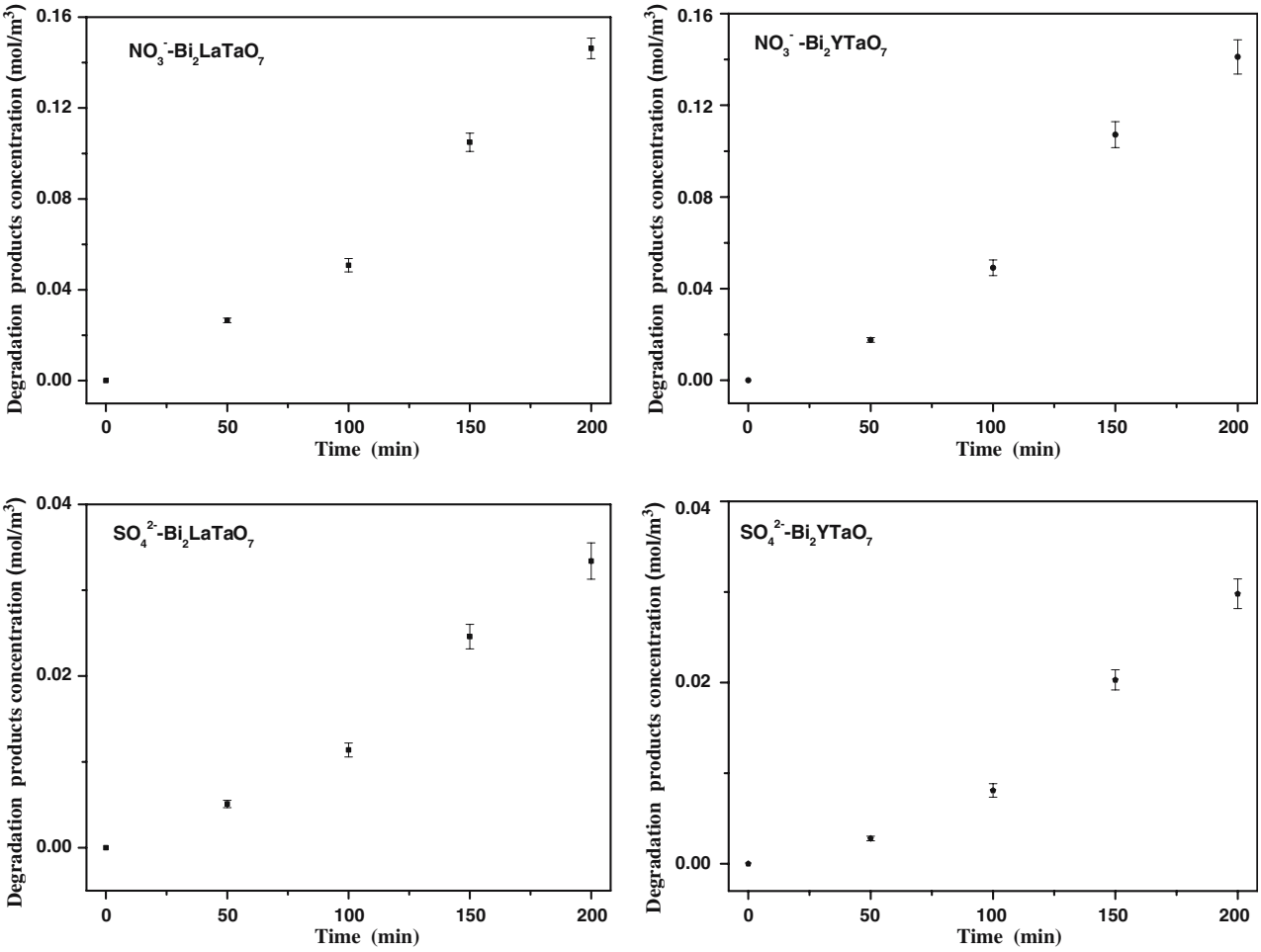

Fig. 9 Evolution of SO_4^{2-} and NO_3^- ions in the solution with the Bi_2MTaO_7 (M = Y and La) photocatalysts during the photocatalytic degradation of MB under visible light irradiation

H_2 and oxidation of H_2O to O_2, respectively. Figure 13 shows suggested band structures of Bi_2MTaO_7 (M = Y and La). Recently, the electronic structures of $InMO_4$ (M = V, Nb and Ta) and $BiVO_4$ were reported by Oshikiri et al. based on the first principles calculations [32]. The conduction bands of the $InMO_4$ (M = V, Nb and Ta) photocatalysts are mainly composed of a dominant d orbital component from V 3d, Nb 4d and Ta 5d orbitals, respectively. The valence bands of the $BiVO_4$ photocatalyst are composed of a small Bi 6s orbital component and a dominant O 2p orbital component. The band structures and valence band levels of Bi_2MTaO_7 (M = Y and La) should be similar to $InMO_4$ (M = V, Nb and Ta) and $BiVO_4$ due to their similar distorted pyrochlore-type structure. Therefore, we conclude that the Bi_2YTaO_7 photocatalyst owns two conduction bands: one is consisted of Ta 5d and the other should be consisted of Y 4d. The valence band of Bi_2YTaO_7 is consisted of a small Bi 6s orbital component and a dominant O 2p orbital component. Similarly, the Bi_2LaTaO_7 photocatalyst owns two conduction bands: one should be composed of Ta 5d and the other should be composed of La 5d. The valence band of Bi_2LaTaO_7 is almost the same as that of Bi_2YTaO_7.

These photocatalysts consist of a three-dimensional network structure of corner-linked MO_6 (M = Y, La and Ta) octahedra and the MO_6 octahedra are connected into chains with Bi^{3+} ions. The shapes of AO_8 and BO_6 polyhedra vary with the O(48f) parameter x in the pyrochlore-type $A_2B_2O_7$ structure. The O(48f) parameter x is 0.375 when the O(48f) atoms are located at the position of the related fluorite-type structure [33]. Thus, information on the lattice distortion can be obtained from the O(48f) parameter x in the pyrochlore-type $A_2B_2O_7$ structure. The lattice distortion is defined according to the distortion of BO_6 polyhedral from the regular octahedral. The O(48f) parameter x of these photocatalysts were attained from the Rietveld structure refinement and the results are described in

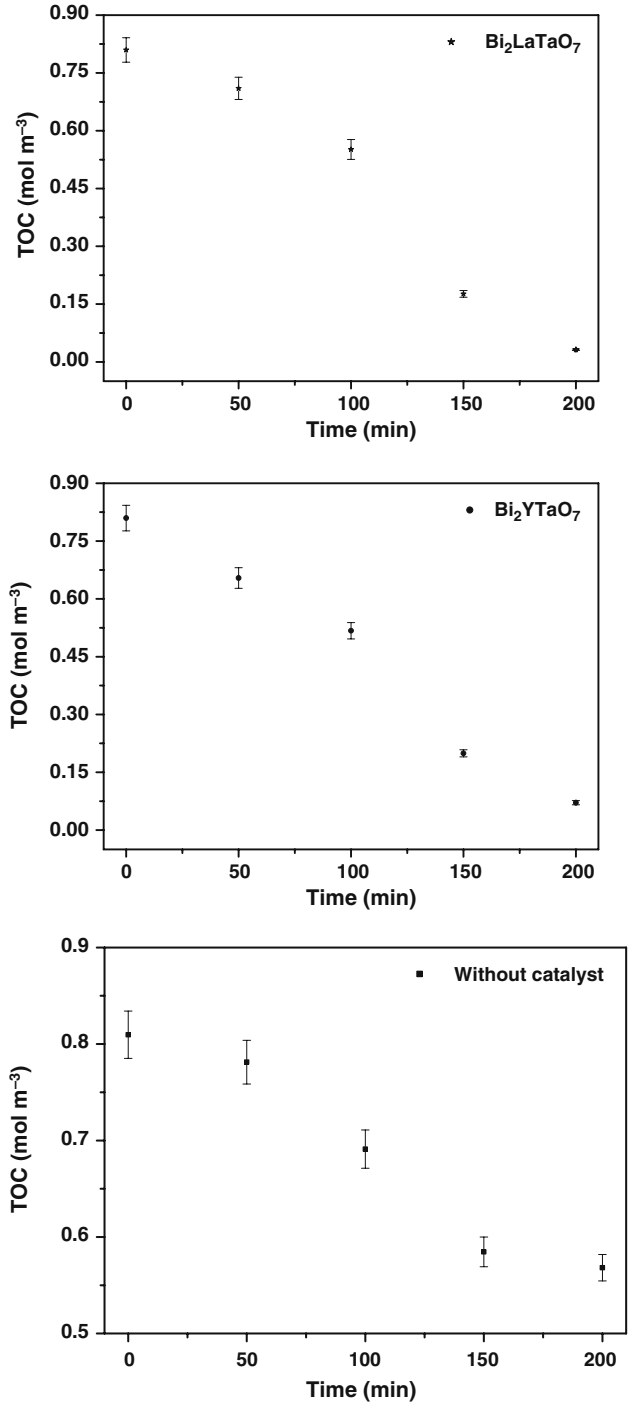

Fig. 10 Disappearance of total organic carbon (TOC) during the photocatalytic degradation of MB by photochemistry (without Bi_2MTaO_7 (M = Y and La)) and by photocatalysis (with Bi_2MTaO_7 (M = Y and La)) under visible light irradiation

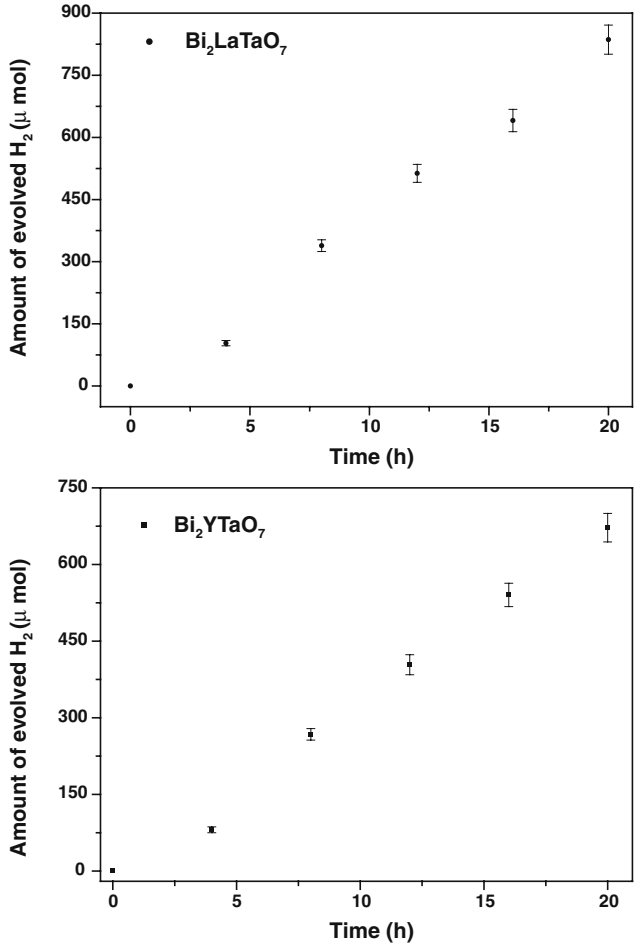

Fig. 11 Photocatalytic H_2 evolution over Bi_2MTaO_7 (M = Y and La) from pure water under ultraviolet light irradiation. (Wavelength: λ = 390 nm, Catalyst: 1 g, H_2O: 300 mL, Light source: 400 W high-pressure Hg lamp.)

Table 3. The lattice distortion was estimated to be 0.070(7) for Bi_2LaTaO_7 and 0.030(3) for Bi_2YTaO_7 because the lattice distortion is equal to 0.375—the O(48f) parameter x. During the process of photocatalytic water splitting into H_2 and O_2, charge separation is necessary to inhibit the recombination of the photoinduced electrons and holes. The lattice distortion is one important parameter for charge separation, and will result in the enhanced photocatalytic activity [34, 12]. In other words, for the photocatalysts with same crystal and electronic structure, the higher photocatalytic activity is mainly resulted from the larger lattice distortion. This conclusion is confirmed by the fact that Bi_2LaTaO_7 with larger lattice distortion (0.070(7)) shows higher photocatalytic activity compared to Bi_2YTaO_7 with the lattice distortion of 0.030(3).

The research on the luminescent properties has given a conclusion that the closer the angle between the corner-linked octahedral is to 180°, the more the excited state is delocalized [35]. This indicates that the photoinduced electrons and holes can move easily if the angle between the corner-linked octahedral is close to 180°. The mobility of the photoinduced electrons and holes also influences the photocatalytic activity

Table 3 Physical properties and formation rates of H_2 or O_2 evolutions from pure water over Bi_2M (M = La and Y)TaO_7

Catalyst	Lattice[a] parameter (Å)	Lattice[b] distortion	M–O1–M angle[c] (°)	Band gap (eV)	Surface area (m^2 g^{-1})	Rate of gas (μ mol h^{-1})	
						H_2^d	O_2^d
Bi_2LaTaO_7	10.9600(2)	0.070(7)	145.8(7)	2.17(3)	1.4(5)	41.8	20.5
Bi_2YTaO_7	10.7859(9)	0.030(3)	97.3(9)	2.22(7)	1.5(6)	33.6	16.0

[a] The lattice parameter was obtained by the Rietveld structure refinement

[b] Lattice distortion was defined as 0.375—the O(48f) parameter *x*

[c] Angle between the corner-linked MO_6 (M = La, Y and Ta) polyhedral

[d] Measured by a 400 W Hg lamp (catalyst: 1.0 g; pure water: 300 mL; non-co-catalyst was loaded onto the catalyst surface)

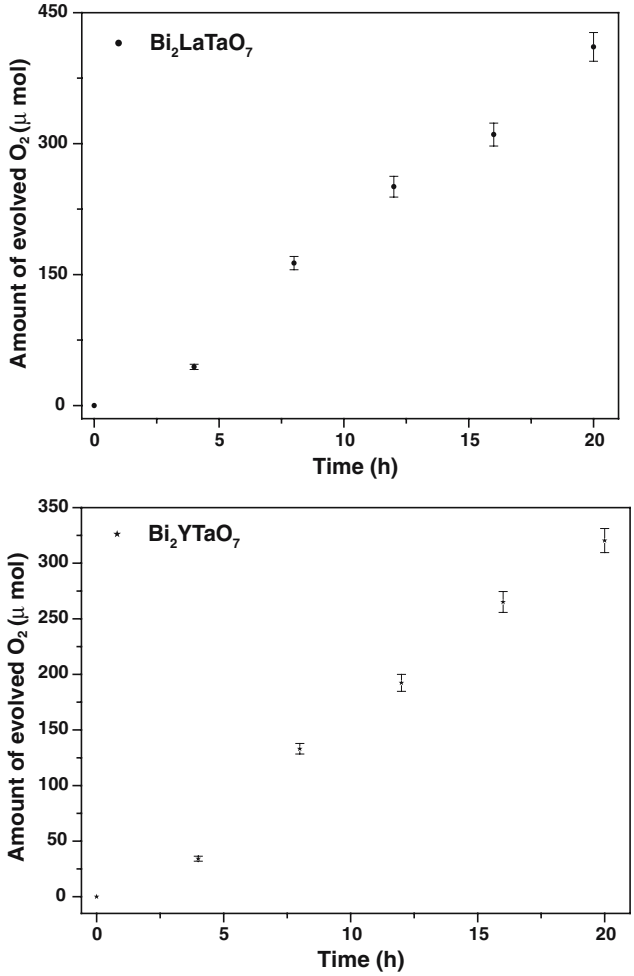

Fig. 12 Photocatalytic O_2 evolution over Bi_2MTaO_7 (M = Y and La) from pure water under ultraviolet light irradiation. (Wavelength: λ = 390 nm, Catalyst: 1 g, H_2O: 300 mL, Light source: 400 W high-pressure Hg lamp.)

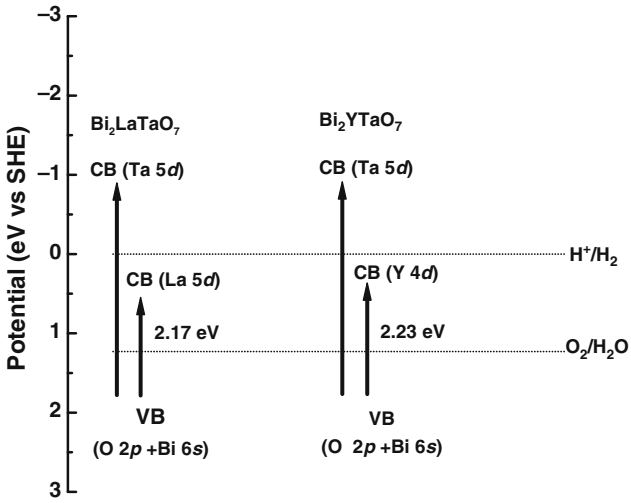

Fig. 13 Suggested band structures of the Bi_2MTaO_7 (M = Y and La) photocatalysts

because it influences the probability of electrons and holes to reach reaction sites on the catalyst surface. The angles between the corner-linked MO_6 (M = La, Y and Ta) octahedral, i.e. the M–O1–M bond angles were attained by the Rietveld structure refinement and the results are shown in Table 3. Comparing the M–O1–M bond angles and the photocatalytic activities of Bi_2LaTaO_7 with those of Bi_2YTaO_7, we can find that the closer the M–O1–M bond angle is to 180°, the higher the photocatalytic activity is. The crystal structures of these photocatalysts are almost the same, but their electronic structures are considered to be different. For the Bi_2MTaO_7 (M = Y and La) photocatalysts, La is a 5d-block metal element and Y is 4d-block metal element, indicating that the photocatalytic activity may be affected by not only the crystal structure but also the electronic structure of the photocatalysts. Both of the lattice distortion and the angles between the corner-linked MO_6 (M = La, Y and Ta) octahedral are possible to influence the photocatalytic activities of Bi_2MTaO_7 (M = La and Y). Although direct absorption of photons by the semiconductor oxide can produce electron–hole pairs in the catalysts, the gases evolution (H_2 or O_2) can not be observed from pure water under visible light irradiation in our

experiments, possibly indicating that the larger energy than the band gap is necessary for splitting water into H_2 and O_2 by photocatalysis.

Conclusions

We prepared single phase of the Bi_2MTaO_7 (M = Y and La) photocatalysts by solid state reaction method and investigated the structural, optical absorption and photocatalytic properties. XRD results indicated that these compounds crystallize in the pyrochlore-type structure, cubic system with space group Fd-3 m. The lattice parameters of Bi_2LaTaO_7 and Bi_2YTaO_7 are 10.9600(2) and 10.7859(9) Å, respectively. The band gaps of Bi_2LaTaO_7 and Bi_2YTaO_7 were estimated to be about 2.17(3) and 2.22(7) eV and the compounds show strong optical absorption in the visible region ($\lambda > 420$ nm). In addition, H_2 or O_2 evolution was observed from pure water respectively with Bi_2MTaO_7 (M = Y and La) as the photocatalysts under ultraviolet light irradiation. In the presence of Bi_2MTaO_7 (M = Y and La), photocatalytic decomposition of aqueous MB could be achieved under visible light irradiation. At the same time, the mineralization of aqueous MB led to the generation of SO_4^{2-} and NO_3^- and to the marked decrease of TOC during the reaction, which suggests that Bi_2MTaO_7 (M = Y and La)/VIS system may be regarded as an effective method for treatment of the wastewater from the textile industry.

Acknowledgement This work was supported by a grant from the Natural Science Foundation of Jiangsu Province (No. BK2006130).

References

1. Honda K, Fujishima A (1972) Nature 238:37
2. Zou Z, Ye J, Sayama K, Arakawa H (2001) Nature 414:625
3. Zou Z, Ye J, Arakawa H (2002) J Phys Chem B 106:13098
4. Zou Z, Ye J, Arakawa H (2000) J Mater Sci Lett 19:1909
5. Anpo M, Takeuchi M (2003) J Catal 216:505
6. Malato S, Blanco J, Cáceres J, Fernández-Alba AR, Agüera A, Rodríguez A (2002) Catal Today 76:209
7. Kodama T, Isobe Y, Kondoh Y, Yamaguchi S, Shimizu KI (2004) Energy 29:895
8. Guan GQ, Kida T, Yoshida A (2003) Appl Catal B: Environ 41:387
9. Guan GQ, Kida T, Harada T, Isayama M, Yoshida A (2003) Appl Catal A: General 249:11
10. Zou Z, Ye J, Arakawa H (2001) Chem Mater 13:1765
11. Zou Z, Ye J, Arakawa H (2002) J Phys Chem B 106:517
12. Kudo A, Kato H, Nakagawa S (2000) J Phys Chem B 104:571
13. Zou Z, Ye J, Arakawa H (2000) Chem Phys Lett 332:271
14. Zou Z, Ye J, Oka K, Nishihara Y (1998) Phys Rev Lett 80:1074
15. Tang J, Zou Z, Yin J, Ye J (2003) Chem Phys Lett 382:175
16. Matos J, Laine J, Herrmann JM (2001) J Catal 200:10
17. Qu P, Zhao J, Shen T, Hidaka H (1998) J Mol Catal A 129:257
18. Xu YM, Langford CH (2001) Langmuir 17:897
19. Asahi R, Morikawa T, Ohwaki T, Aoki K, Taga Y (2001) Science 293:269
20. Li FB, Li XZ (2002) Appl Catal A 228:15
21. Li FB, Li XZ (2002) Chemosphere 48:1103
22. Kramer MJ, Dennis KW, Falzgraf D, Mccallum RW, Malik SK, Yelon WB (1997) Phys Rev B 56:5512
23. Tung LC, Chen JC, Wu MK, Guan W (1999) Phys Rev B 59:4504
24. Bernard D, Pannetier J, Lucas J (1978) Ferroelectrics 21:429
25. Golovshchikove GI, Isupov VA, Tutov AG, Nikove AG, Myl IE, Nikitina PA, Tulinova OI (1973) Sov Phys Solid State 14:2539
26. Izumi F, Crystallogr J (1985) Assoc Jpn 27:23
27. Xu J, Emge T, Ramanujachary KV, Hohn P, Greenblatt M (1996) J Solid State Chem 125:192
28. Butler MA (1977) J Appl Phys 48:1914
29. Tauc J, Grigorovici R, Vancu A (1966) Phys Stat Sol 15:627
30. Wang JH, Zou ZG, Ye JH (2003) *Functionally Graded Materials VII Materials Science Forum* 423:485
31. Lachheb H, Puzenat E, Houas A, Ksibi M, Elaloui E, Guilard C, Herrmann JM (2002) Appl Catal B 39:75
32. Oshikiri M, Boero M, Ye J, Zou Z, Kido G (2002) J Chem Phys 117:7313
33. Subramanian MA, Aravamudan G, Subba Rao GV (1983) Prog Solid State Chem 15:55
34. Inoue Y, Kohno M, Ogura S, Sato K (1997) Chem Phys Lett 267:72
35. Wiegel M, Middel W, Blasse G (1995) J Mater Chem 5:981